SPE 95841

Near-Wellbore Alteration and Formation Stress Parameters Using Borehole Sonic Data

B. Sinha, SPE, T. Bratton, SPE, J. Cryer, and S. Nieting, Schlumberger OFS, and G. Ugueto, A. Bakulin, SPE, and M. Hauser, Shell E&P Co.

This paper was prepared for presentation at the 2005 SPE Annual Technical Conference and Exhibition held in Dallas, Texas, U.S.A., 9 – 12 October 2005.

Abstract

Highly depleted reservoirs exhibit sharply lower pore pressures and horizontal stress magnitudes than in the overlying shaly formation. Drilling through such depleted reservoirs can cause severe fluid loss and drilling-induced wellbore instability. Accurate and reliable estimates of horizontal stresses can provide early warning of impending drilling problems that may be mitigated by appropriate drilling fluid design and drilling practices. We have developed a new multi-frequency inversion algorithm for the estimation of maximum and minimum horizontal stress magnitudes using cross-dipole dispersions. Borehole sonic data for the case study presented in this paper was acquired by a cross-dipole sonic tool in a deep-water well, offshore Louisiana in the Gulf of Mexico (GOM). The logged interval spans 1000 ft below the casing shoe. In addition, the Modular Dynamic Tester (MDT)[1] mini-frac tests were performed at three depths in shale, yielding two minimum horizontal stress magnitudes. The borehole sonic data was suitable for inversion of cross-dipole dispersions at three depths in shale and also at a depth in a highly depleted sand reservoir. There was one depth in shale above the depleted sand where we could estimate the minimum horizontal stress magnitude using both the MDT mini-frac tests and inversion of borehole sonic data. The results of the two techniques are consistent, providing encouragement for further validation of the multi-frequency inversion of cross-dipole dispersions to estimate horizontal stresses. Even though the overburden stress is expected to increase with depth, both the maximum (SHmax) and minimum (Shmin) horizontal stresses obtained from the inversion of borehole sonic data are significantly smaller in the depleted sand than in the overburden shale. However, both the horizontal stress magnitudes increase again in the shale below the depleted sand. Such rapid variations in horizontal stress magnitudes cause large fluctuations in the safe mud weight window. This challenge in drilling through the depleted sand was successfully handled by using special drilling fluid to mitigate seepage losses and differential sticking in the depleted sand and overlying shale. We have also performed Dipole Radial Profiling (DRP) of formation shear slownesses using the measured cross-dipole dispersions at three depths in shale and one in the highly depleted sand. Analysis of radial profiles in the two orthogonal directions indicates plastic yielding or stiffening of rock in the near-wellbore region. While plastic yielding increases the shear slowness, stiffening would reduce the shear slowness.

Introduction

Formation stresses play an important role in geophysical prospecting and development of oil and gas reservoirs. Both the direction and magnitude of these stresses are required in (a) planning for borehole stability during directional drilling, (b) hydraulic fracturing for enhanced production, and (c) selective perforation for prevention of sanding during production. Wellbores drilled through base salt in the GOM are subject to increased risks of hole closure that might be attributed to complex and rapidly varying formation stresses. In addition, drilling through highly pressure depleted reservoirs raises considerable risks of excessive mud loss, internal blowout and differential sticking.[1] Drilling through such depleted sands was accomplished in the Ursa field in the GOM using water-based mud with monomer and resin materials that exhibit larger fracture propagation pressure than that of oil-based mud – even though the fracture opening pressures are similar for both the water-based and oil-based mud.

The formation stress state is characterized by the magnitude and direction of three principal stresses. Figure 1 shows a schematic diagram of a vertical borehole in a formation subject to the three principal stresses. Generally, the overburden stress (S_V) is reliably obtained by integrating the formation mass density from the surface to the depth of interest. Consequently, estimating the other two principal

[1] Mark of Schlumberger

stresses (SHmax and Shmin) in the horizontal plane is the remaining task necessary to fully characterize the formation stress state.

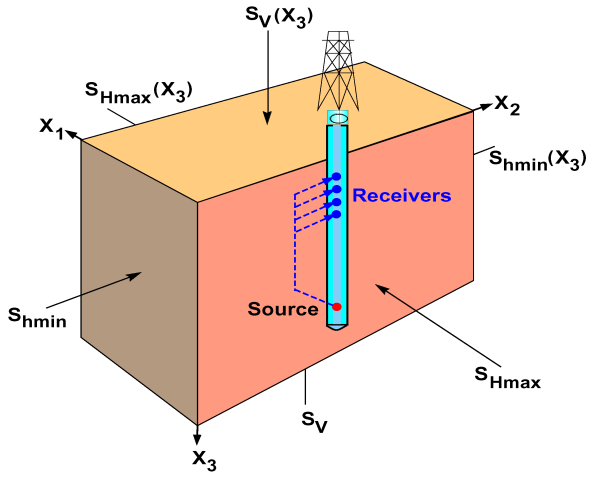

Fig. 1–Schematic of a borehole in the presence of formation principal stresses with the borehole axis parallel to the overburden stress.

Existing techniques for the estimation of horizontal stress magnitudes based on correlations with dynamic Poisson's ratio may not reliably yield the rapid variations in horizontal stresses in different stratigraphic layers.

The Modular Dynamic Tester (MDT), in dual-packer stress testing mode yields the minimum in-situ stress magnitude.[2] Currently, the maximum horizontal stress must be determined from damage mechanics constraints based on borehole breakouts.[3] Estimation of the maximum horizontal stress magnitude remains a challenge in the industry.

Near-wellbore alteration can be caused by several sources, such as borehole stress concentrations, drilling mud pressure, plastic yielding of the rock prior to breakouts, shale swelling, drilling-induced fractures, and invasion of monomer and resin materials in synthetic drilling muds used to strengthen weak formations.[1,4-6] Estimation of the magnitude and radial extent of mechanical alteration helps in an optimal design of perforation tunnel length for improved flow rate in the presence of near-wellbore permeability impairment.

This paper presents a summary of results for the minimum horizontal stress obtained from the micro-hydraulic fracturing technique using the dual-packer module of the MDT tool. Next we describe results from the analysis of cross-dipole sonic data from a post-drill logging program for the well to estimate the formation stress magnitudes and radial extent of near-wellbore alteration. This well was successfully drilled through a highly depleted sand reservoir using a special synthetic mud with substantially less fluid loss than typical muds. In the sands, we infer the radial depth of invasion of the monomer and resin components of the mud from the radial profile of shear slowness away from the borehole surface. We also compare results for the minimum horizontal stress magnitudes obtained from the borehole sonic data with those estimated from the mini-frac tests using the MDT dual-packer module in the shales.

Radial profiles of shear slownesses together with annular pressure history can also be used to estimate in-situ UCS of the rock.[7]

Horizontal stress estimates using mini-frac tests

It is generally agreed that the best estimate of minimum in-situ stress is determined using micro-hydraulic fracturing techniques such as that reported by Haimson.[8] Stress measurements were conducted in the Ursa-12 well using the technique described by Desroches and Kurkjian.[2] Three depths were selected for stress testing. While it was desired to determine a closure stress in all three zones, complications prevented the stress measurement in one zone. Specifically, the maximum packer pressure was reached prior to the initiation of a hydraulic fracture.

Figure 2 shows a schematic diagram of the MDT tool with dual-packers for micro-hydraulic fracturing of rock for determining fracture opening and propagation pressures. Both the top and bottom packers are about 3 ft (1 m) in height. The depth interval between them is also about 3 ft.

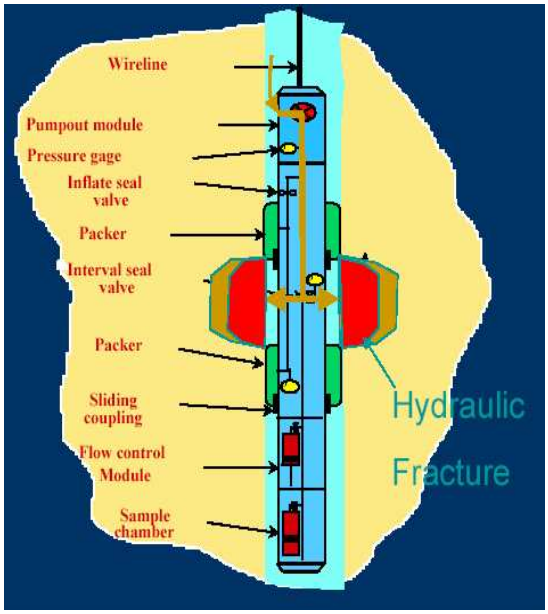

Fig. 2–Schematic diagram of the Modular Dynamic Tester (MDT) with dual packers for micro-hydraulic fracturing of rock for determining fracture opening and propagation pressures.

The interval pressure is monitored during the pump-in for a reasonably uniform flow rate. Figure 3a shows a plot of the initial breakdown in one test while Figure 3b displays the final closure. Figure 3a shows the interval pressure, the borehole pressure measured between the upper and lower sealing packer elements, as a function of the volume of pumped fluid. Fracture initiation is indicated by the divergence from a straight-line pressure increase (given a substantially constant pump rate), and uncontrolled fracture propagation is indicated by a decrease in interval pressure. These two observations support the diagnosis of a created fracture. The interval pressure can increase after breakdown for different reasons, (e.g., the fracture is likely to be confined in height and/or leak-off is limited by the formation permeability).

Figure 3b displays the interval pressure as a function of time during a controlled flowback. A flowback test was executed to determine closure pressure due to the likelihood a newly created open fracture would take hours or even days to close given the low permeability of the formation. An indication of closure is seen at about 13,014 psig. Consequently, our estimate of the minimum horizontal stress magnitude in this test is about 13,014 psi at a measured depth (MD) of 20,080 ft. Closure pressure is less than breakdown pressure because the stress cage surrounding the wellbore often concentrates the far-field stresses at the wellbore wall. The MDT stress testing interpretation at the second depth was identical to the formation response shown in Figs. 3a and 3b, differing only in the absolute magnitude. The results are summarized in the first and third rows of Table 1 for measured depths of 19,832 and 20,080 ft, respectively.

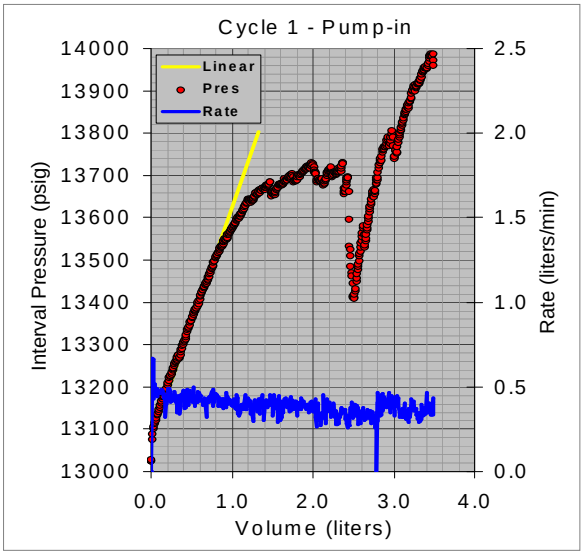

Fig. 3a–Pressure response during the initial pump-in cycle. Note the decrease in pressure indicating unstable fracture growth after pumping 2.4 liters.

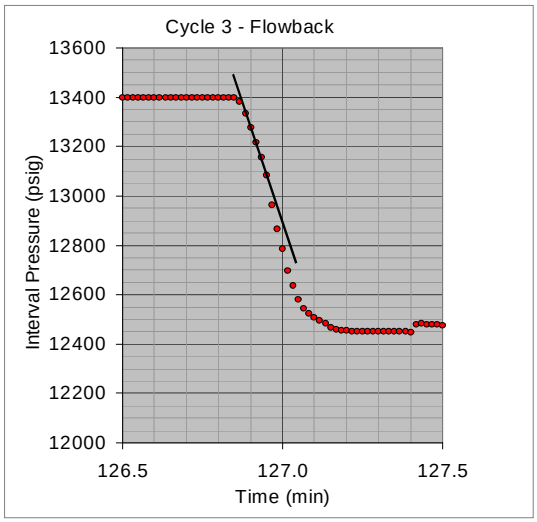

Fig. 3b–Pressure response during a controlled flow-back. The change in slope at about 13,014 psig indicates the closure of the fracture and the minimum in-situ (horizontal) stress

Stress magnitudes using borehole sonic

Sonic velocities in formations change as a function of rock lithology/mineralogy, porosity, clay content, fluid saturation, stresses, and temperature. To estimate changes in the formation stress magnitudes from measured changes in sonic velocities, it is necessary to select a depth interval with a reasonably uniform lithology, clay content, saturation and temperature so that the measured changes in velocities can be related to corresponding changes in formation stress magnitudes. Any change in porosity caused by normal compaction is accounted for by corresponding changes in the formation effective bulk density and stiffnesses. Assuming that the measured changes in sonic velocities are largely caused by changes in stresses, it is possible to invert borehole sonic velocities for the estimation of changes in formation stress magnitudes.[9,10]

The underlying theory behind the estimation of formation stresses using borehole sonic data is based on acoustoelastic effects in rocks. Acoustoelasticity in rocks refers to changes in elastic wave velocities caused by changes in pre-stress in the propagating medium. Elastic wave propagation in a pre-stressed material is described by equations of motion for small dynamic fields superposed on a statically deformed state of the material. These equations are derived from the rotationally invariant equations of nonlinear elasticity. The linear equations of motion for isotropic materials contain two independent elastic stiffnesses that are defined by the dynamic Young's modulus (Y) and Poisson's ratio (ν), or equivalently, the two Lamé parameters, (λ and μ).

The equations of motion for pre-stressed isotropic materials contain three additional elastic stiffness constants (C_{111}, C_{144}, and C_{155}) together with the biasing stresses.[11,12] A forward solution of equations of motion in pre-stressed materials yields plane wave velocities as a function of principal stresses in the propagating medium.The presence of a borehole in a triaxially stressed formation causes near-wellbore stress distributions that can be obtained from linear elastic deformation theory. Near-wellbore stress distributions can be mapped into corresponding sonic velocity distributions provided stress coefficients of velocities are known. The stress coefficients of velocities are defined in terms of formation nonlinear constants referred to a reference state close to the in-situ stress state of the formation. Changes in cross-dipole dispersions caused by near-wellbore stress distributions can be inverted to estimate far-field stresses and formation nonlinear constants.

Flexural wave propagation in a borehole

A dipole source in a fluid-filled borehole primarily generates a dispersive flexural mode whose velocity is a function of frequency. Since the radial depth of investigation varies as a function of frequency of flexural waves, it is possible to invert measured cross-dipole dispersions to obtain radial variations in formation shear velocity along the two orthogonal radial polarizations. Radial variations in formation shear velocity may be caused by near-wellbore stress concentrations as well as by plastic yielding of the rock.[13] Generally, the plastic yielding of the rock is confined to the high stress concentration area close to the borehole surface. In contrast,

radial variations in formation shear velocity caused by near-wellbore stress concentrations extend beyond this plastic zone.

Since the presence of a borehole causes well-defined near-wellbore stress distributions and the associated shear velocity distributions can be measured in terms of frequency-dependent changes in the borehole flexural velocities – also referred to as the borehole flexural dispersion -- it is possible to invert cross-dipole dispersions for the horizontal stress magnitudes together with the formation nonlinear constants.

Effective stresses and the Biot parameter

Elastic wave velocities in porous materials change as a function of effective stresses in the propagating medium. These effective stresses σ_{ij} are defined by

$$\sigma_{ij} = S_{ij} - \alpha\delta_{ij}P_P, \qquad (1)$$

where δ_{ij} is the Kronecker delta and the Biot parameter α is given by

$$\alpha = 1 - \frac{K}{K_S}, \qquad (2)$$

where K is the bulk modulus of the dry aggregate and K_S is the intrinsic bulk modulus of the solid matrix.[14] Even though the porosity effect is not explicit in this expression, it is included in the value of the effective bulk modulus K of the dry aggregate. In the case of a nonporous and impermeable formation, $K \cong K_S$, and $\alpha=0$. In contrast, for natural soils, $K \ll K_S$, and $\alpha=1$. In porous rocks, the Biot parameter is affected by both the porosity, pore shape, and connectivity.[15] Generally, $\phi<\alpha<1$, in porous rocks with porosity ϕ. More importantly, the Biot parameter α_n in a normally compacted shale formation with open pores is typically more than that in an overpressured (α_o) shale with larger effective porosity and closed pores, i.e., $\alpha_n>\alpha_o$.

We have developed a general perturbation model that relates perturbations in the three principal stresses (σ_V, σ_H, and σ_h) from a chosen reference state to fractional changes in the fast and slow flexural velocities at a given wavenumber k_i by

$$\left(\frac{\Delta V_m^{F,S}}{V_m^R}\right)_i = \left(\frac{\partial V_m^{F,S}}{V_m^R \partial\sigma_V}\right)_i \Delta\sigma_V + \left(\frac{\partial V_m^{F,S}}{V_m^R \partial\sigma_H}\right)_i \Delta\sigma_H + \left(\frac{\partial V_m^{F,S}}{V_m^R \partial\sigma_h}\right)_i \Delta\sigma_h, \qquad (3)$$

where the stress coefficient of velocity at a given wavenumber k_i is given by

$$\left(\frac{\partial V_m^{F,S}}{V_m^R \partial\sigma_j}\right)_i = L_{mj}^i + M_{mj}^i \frac{C_{111}}{\mu} + N_{mj}^i \frac{C_{155}}{\mu} + P_{mj}^i \frac{C_{144}}{\mu}, \qquad (4)$$

and the subscript m denotes one of the two orthogonal flexural modes (m=1, 2, respectively, refers to the fast- and slow-flexural modes), and the index j represents one of the three effective principal stresses σ_V, σ_H, and σ_h (j=1 $\rightarrow \sigma_V$; j=2 $\rightarrow \sigma_H$; j=3 $\rightarrow \sigma_h$). The superscripts F and S, respectively, denote the fast- and slow-flexural wave velocities; and R refers to the flexural wave velocity in the chosen reference state. The fast- and slow-flexural waves have radial polarization parallel and perpendicular to the maximum horizontal (σ_H) stress direction, respectively. The four sensitivity coefficients L^i_{mj}, M^i_{mj}, N^i_{mj}, and P^i_{mj} are sensitivity integrals evaluated in terms of flexural solution at a given wavenumber k_i in the reference state. C_{111}, C_{144}, and C_{155} are the three independent nonlinear constants and μ is the horizontal shear modulus in the reference state. We determine the shear modulus in the reference state from the Stoneley velocity at the reference depth.

Inversion of dipole dispersions for formation stresses

When cross-dipole waveforms produce wideband dispersions exhibiting crossovers, a procedure for the estimation of maximum (S_H) and minimum (S_h) horizontal stresses consists of the following steps:

1. Select a reference depth in a reasonably uniform lithology interval where cross-dipole dispersions exhibit a crossover.
2. Estimate an effective Young's modulus and Poisson's ratio in the borehole cross-sectional plane using the compressional and shear moduli from sonic velocities. These elastic moduli are used to calculate static deformation of the formation surrounding a borehole.
3. Calculate a reference flexural dispersion for an assumed homogeneous formation using the measured compressional velocity V_P , a chosen shear velocity V_R rather close to the slow-shear velocity in the far-field, formation bulk mass density ρ_b, mud mass density ρ_f, mud compressional velocity V_f, and borehole radius a.
4. Compute the sensitivity coefficients L^i_{mj}, M^i_{mj}, N^i_{mj}, and P^i_{mj} as a function of wavenumber k_i , for both the fast and slow flexural waves in the chosen reference state in step 3. These coefficients are calculated in terms of the flexural wave eigensolution in the reference state and static deformation of the formation caused by near-wellbore stress distributions.
5. Define a cost function ε from differences in the fast- and slow-flexural velocities and sensitivity coefficients at various wavenumbers k_i, and unknown formation nonlinear constants and stress magnitudes. Figure 4 shows the velocity differences as a function of wavenumber that are needed in the expression for the cost function ε defined below:

$$\begin{aligned}\varepsilon = \sum_{i=1}^{n} \frac{(V_i^F - V_i^S)}{V_i^R} &- (L_{12}^i - L_{22}^i)\Delta\sigma_H - (L_{13}^i - L_{23}^i)\Delta\sigma_h \\ &- (M_{12}^i - M_{22}^i)\frac{C_{111}}{\mu}\Delta\sigma_H - (N_{12}^i - N_{22}^i)\frac{C_{155}}{\mu}\Delta\sigma_H \\ &- (P_{12}^i - P_{22}^i)\frac{C_{144}}{\mu}\Delta\sigma_H \\ &- (M_{13}^i - M_{23}^i)\frac{C_{111}}{\mu}\Delta\sigma_h - (N_{13}^i - N_{23}^i)\frac{C_{155}}{\mu}\Delta\sigma_h \\ &- (P_{13}^i - P_{23}^i)\frac{C_{144}}{\mu}\Delta\sigma_h, \end{aligned} \qquad (5)$$

where i=1,2,3,…n are the axial wavenumbers (or frequencies) where the measured velocity differences $(V_i^F-V_i^S)/V_i^R$ are calculated.

6. Solve for the horizontal stress magnitudes $\Delta\sigma_H$ and $\Delta\sigma_h$, together with the nonlinear parameters C_{111}/μ, C_{155}/μ, and C_{144}/μ from a nonlinear least-squares minimization of the cost function ε defined in step 5.

Estimation of these stress parameters requires an iterative process to make sure that estimated stresses satisfy the constraints based on observed borehole failures. These constraints may be based on tensile failures during mini-frac tests or breakouts for the wellbore pressure, estimated rock coefficient of friction, tensile strength and confined compressive strength.[16]

Formation stresses from sonic data

Estimation of formation stress magnitudes starts from a standard processing of cross-dipole sonic data that helps in identifying depth intervals that exhibit shear-slowness anisotropy. Figure 5 shows a cross-dipole sonic log in a shale interval that includes the MDT mini-frac test location shown by the red arrow in the depth track. At this location, we notice evidence of shear slowness anisotropy and the fast-shear azimuth is approximately NW20.

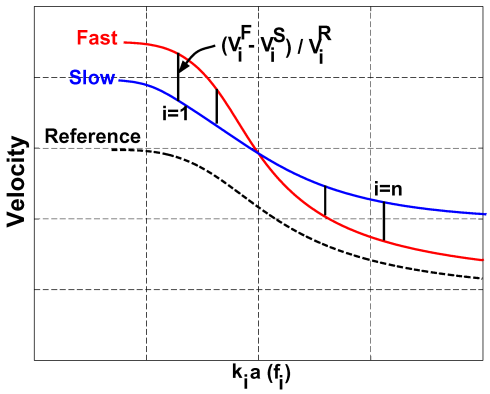

Fig. 4–Schematic of the fast-, slow-, and reference-flexural velocity dispersions. Normalized differences between the fast- and slow-flexural velocities at various wavenumbers are input to the inversion model for the estimation of horizontal stress magnitudes.

Next we process the recorded waveforms for estimating dipole dispersions and look for an evidence of crossovers as an indicator of horizontal stress-induced shear anisotropy dominating the data.

In Fig. 6 the red and blue circles denote the fast and slow dipole dispersions obtained from the recorded cross-dipole waveforms in a shale interval at depth 20078.5 ft. The measured dipole dispersions exhibit a crossover around 3.5 kHz indicating stress-induced shear slowness anisotropy dominating the data. The red and blue curves are theoretical dispersions calculated for the two assumed homogeneous and isotropic formations with formation shear slownesses of 205 and 215 μs/ft, respectively. The formation mass density and compressional slowness are assumed to be the same for the two cases. The compressional slowness of the synthetic mud is estimated to be 220 μs/ft.

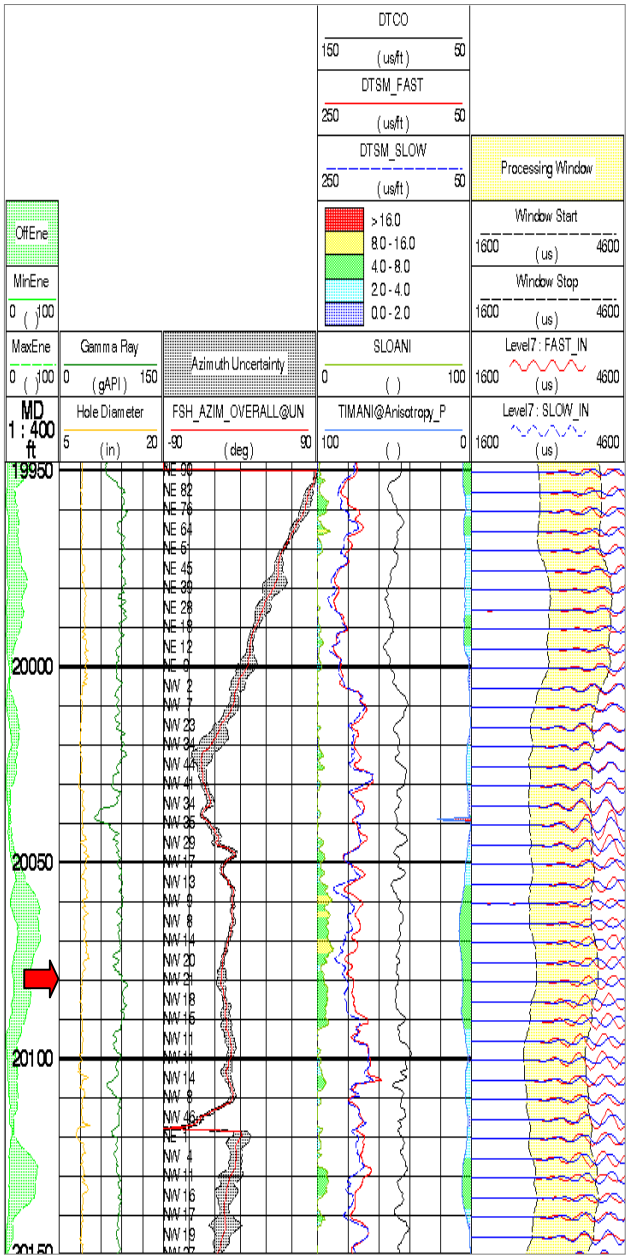

Fig. 5–Cross-dipole sonic logs. The green shaded area in the depth trackdenotes differences between the maximum and minimum energies in the cross-component. The first track contains the gamma ray (green line). The next three tracks show, respectively, the fast-shear direction measured from the north; the compressional, fast-, and slow-shear slowness logs; and the processing window used to obtain the fast-shear azimuth.

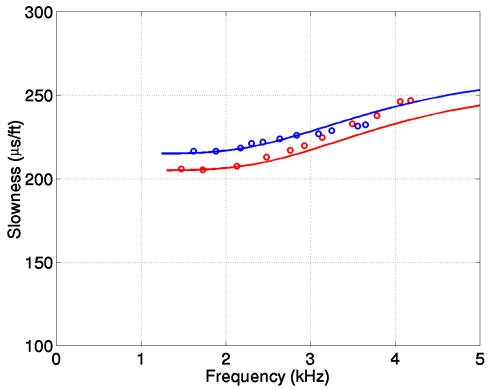

Fig. 6–Measured fast (red circles) and slow (blue circles) flexural dispersions obtained from cross-dipole sonic waveforms at measured depth (MD) of 20,078.5 ft. The red and blue solid curves denote theoretical dipole dispersions for the two effective homogeneous and isotropic formations with the fast and slow shear slownesses, respectively.

We invert differences between the measured fast and slow dipole dispersions (denoted by the red and blue circles) at several frequencies for the effective horizontal stress magnitudes together with the three formation nonlinear constants referred to a chosen reference state. The inversion is based on an iterative nonlinear least-squares minimization algorithm. To check convergence of the inverted stress magnitudes and nonlinear constants, we compare in Fig. 7 the predicted and measured differences in the fast and slow flexural slownesses at various frequencies. The predicted flexural slownesses have been obtained from equation (3) using the estimated formation stress magnitudes and stress-coefficients of fast and slow flexural velocities. Good agreement between the predicted and measured values confirms a successful inversion of dipole dispersions for formation stress parameters.

Near-wellbore stress distributions have been calculated based on linear elasticity using the wellbore pressure, pore pressure together with the estimated formation principal stresses at measured depth of 20,078.5 ft. Figures 8a and 8b, respectively, display the axial, radial and hoop stress

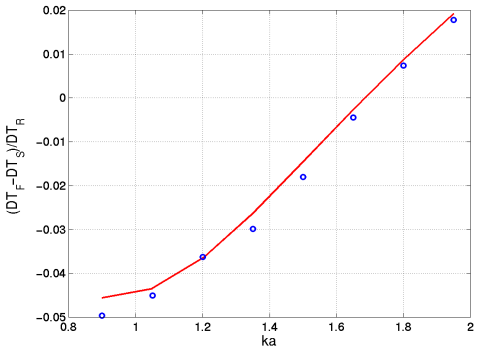

Fig. 7–MD 20,078.5 ft: Comparison of predicted (red curve) and measured (blue circles) differences between the fast and slow dipole dispersions at various normalized wavenumbers.

distributions as a function of radial position away from the borehole surface along the maximum and minimum horizontal stress azimuths. These stress distributions have been obtained using estimated values of the far-field formation stresses. To constrain the estimated stress magnitudes, we assume that the earth stresses at a given depth cannot exceed the frictional strength of existing faults.[16] Consequently, we check for the consistency of estimated horizontal stress magnitudes against allowable stresses within the stress polygon constructed based on Coulomb and Anderson faulting theories. Coulomb faulting theory predicts the difference between the maximum and minimum principal stresses in terms of frictional strength of faulted (failed) rock at a given depth and pore pressure. Anderson faulting theory helps in defining relative stress magnitudes. Following Jaeger and Cook[17], we know that for normal faulting

$$\frac{\sigma_1}{\sigma_3} = \frac{S_V - P_P}{S_{h\min} - P_P} \le \left[(\mu_f^2 + 1)^{1/2} + \mu_f \right]^2, \quad (6)$$

where μ_f is the coefficient of friction of the earth's crust at the chosen depth. Figure 9a displays the stress polygon based on the Coulomb's frictional equilibrium condition for the assumed coefficient of friction of 0.5. The location of the red circle denotes the estimated values of SHmax and Shmin. The dashed blue and red lines denote the tensile strength and confined compressive strength of 0.1 kpsi and 6.5 kpsi, respectively. If the estimated stresses exceed these threshold, tensile fracture and breakout would occur at the borehole surface. The estimated stresses denoted by X are slightly below the threshold implying absence of any borehole failure for the wellbore pressure at this depth.

Figure 9b illustrates changes in the tensile fracture (dashed blue line) and breakout threshold (dashed red line) caused by an increase in the wellbore pressure P_W to 13.7 kpsi. Notice that the estimated stresses denoted by X is now on the dashed blue line indicating a tensile strength of 0.1 kpsi. This implies that an increase of P_W to 13.7 kpsi would initiate tensile fracture at the borehole surface. This is close to the observed fracture opening pressure of about 13.6 kpsi at MD of 20,080 ft during the mini-frac tests using the dual-packer module of the MDT tool.

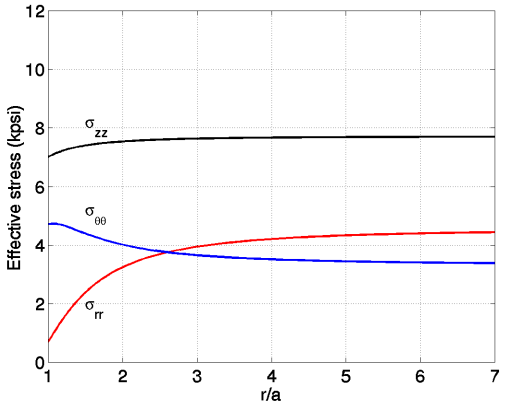

Fig. 8a–Radial variation of axial (σ_{zz}), hoop ($\sigma_{\theta\theta}$), and radial (σ_{rr}) effective stresses at an azimuth parallel to the maximum horizontal stress direction at depth 20,078.5 ft. Notice that the largest differential stress at the borehole surface (r/a=1) is about 7 kpsi.

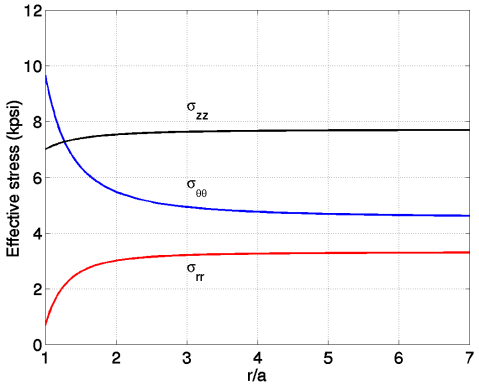

Fig. 8b–Radial variation of axial (σ_{zz}), hoop ($\sigma_{\theta\theta}$), and radial (σ_{rr}) effective stresses at an azimuth perpendicular to the maximum horizontal stress direction. Notice that the largest differential stress at the borehole surface (r/a=1) is about 9.5 kpsi.

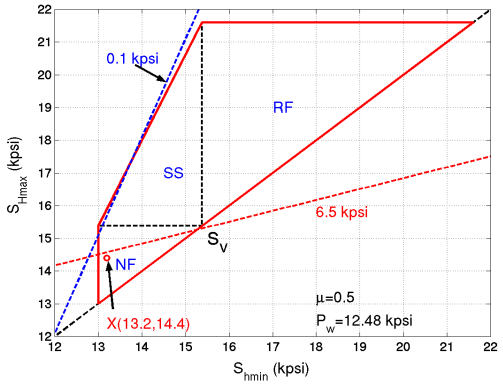

Fig. 9a–Stress polygon that constrains possible magnitudes of S_{hmin} and S_{Hmax} at a given depth with overburden stress S_V, pore pressure P_P, wellbore pressure P_W, and an assumed Coulomb's coefficient of friction μ_f=0.5. The dashed blue and red lines, respectively, represent the assumed tensile strength of 0.1 kpsi; and compressive strength of 6.5 kpsi, and wellbore pressure P_W=12.48 kpsi at this measured depth of 20,078.5 ft. Estimated values of S_{hmin} =13.2, and S_{Hmax}=14.4 kpsi using cross-dipole sonic data.

The red curve in Fig. 10 shows the azimuthal variation of the effective hoop stress ($\sigma_{\theta\theta}$) for the estimated formation stresses, pore pressure, and wellbore pressure P_W =13.7 kpsi. The dashed blue line represents rock tensile strength of 0.1 kpsi. These results predict the initiation of tensile fracture at a wellbore pressure of 13.7 kpsi which is consistent with the observed breakdown pressure at the measured depth of 20,080 ft during the mini-frac tests performed with the dual-packer module of the MDT tool.

Table 1 contains a summary of estimated maximum (SHmax) and minimum (Shmin) horizontal stress magnitudes obtained from measured cross-dipole dispersions at four depths where they exhibit crossovers and the data quality is suitable for inversion for stresses. The overburden stress Sv and pore pressure PP are input to the inversion algorithm. The first and third rows, respectively, in Table 1 show estimated values of Shmin obtained from the mini-frac tests performed at measured depths of 19,832 and 20,080 ft in the overlying shale. Good agreement is observed between the Shmin magnitude obtained from the mini-frac tests at 20,080 ft and cross-dipole sonic data at a nearby depth of 20078.5 ft (MD).

Table 1: SHmax and Shmin magnitudes

MD (ft)	TVD (ft)	SV (psi)	SHmax (psi)	Shmin (psi)	Pp (psi)
19832.0	17733.0	15126		12539	10994
20078.5	17979.4	15381	14472	13234	11531
20080.0	17980.9	15382		13014	11531
20540.0	18440.4	15864	11197	9295	8639
20599.0	18499.3	15925	15175	13151	11778
20658.5	18558.5	15987	14993	12962	11821

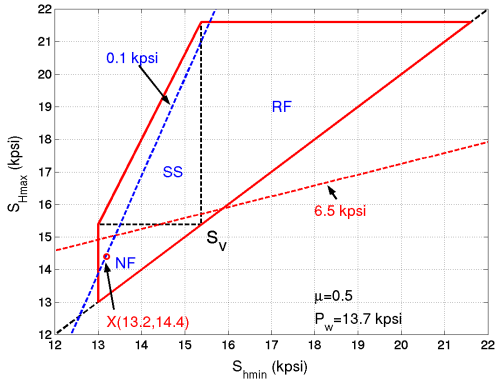

Fig. 9b–MD 20,078.5 ft: Stress polygon that constrains possible magnitudes of S_{hmin} and S_{Hmax} at a given depth with overburden stress S_V, pore pressure P_P, wellbore pressure P_W, and an assumed Coulomb's coefficient of friction μ_f=0.5. Estimated values of S_{hmin} =13.2 kpsi, and S_{Hmax}=14.4 kpsi using cross-dipole sonic data.

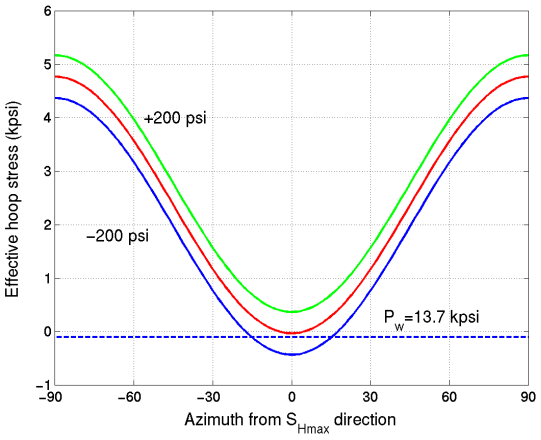

Fig. 10–The red curve shows radial variation of effective hoop ($\sigma_{\theta\theta}$) stress for the estimated horizontal stress magnitudes (S_{hmin} =13.2, and S_{Hmax}=14.4 kpsi), pore pressure, and the wellbore pressure P_W=13.7 kpsi at measured depth of 20,078.5 ft. The green and blue curves display radial variations of the hoop stress for horizontal stresses of 200 psi larger and smaller than those estimated from the cross-dipole sonic data. The dashed blue line represents rock tensile strength of 0.1 kpsi.

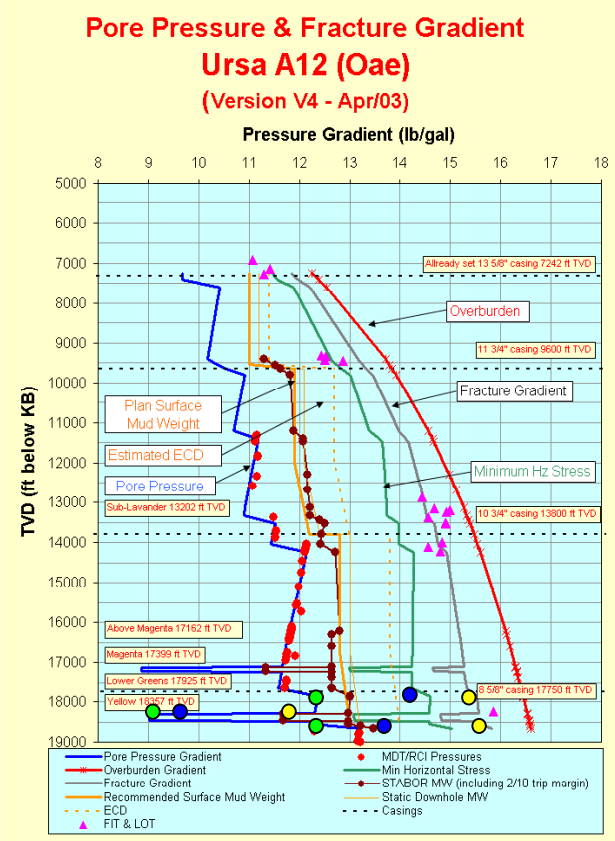

Fig. 11–A geomechanical model of the Ursa A12 well showing the overburden, fracture, pore pressure, and minimum horizontal stress gradients. The solid yellow and blue circles denote the estimated maximum and minimum horizontal stress magnitudes from borehole sonic data. The solid green circle represents the estimated pore pressures at these depths. Estimates shown by solid circles are at TVDs of 17979, 18440, and 18558 ft.

Figure 11 shows a summary of geomechanical properties of the formation obtained from the Ursa-12 well data. The predicted mud weight is obtained from the Shell's proprietary STABOR code used to analyze wellbore stability for assumed formation stresses. The solid red curve shows the overburden stress gradient. The green solid curve denotes the estimated minimum horizontal stress magnitude based on a local Poisson's ratio trend and overburden stress at a given depth. The purple triangles represent the fracture gradients obtained from the formation integrity tests at casing points. The solid yellow and blue circles, respectively, denote the estimated maximum and minimum horizontal stress magnitudes obtained from the inversion of cross-dipole sonic data. The solid green circles represent the pore pressures used in the inversion at the chosen depths. Notice a sharp reduction in the pore pressure in the highly depleted reservoir intervals. In these zones, the static downhole mud weight (shown by solid brown circles) is larger than the minimum horizontal stress that can cause drilling mud loss into the formation. Drilling through such highly depleted reservoirs may be aided by the use of special synthetic drilling mud with high viscosity to reduce fluid loss. The use of monomer and resin materials in water-based mud can strengthen the weak sand and enable successful drilling even in the presence of large overbalance.[1]

Dipole Radial Profiling (DRP) of shear slowness

In this section, we analyze cross-dipole sonic data to estimate stress-induced near-wellbore alteration or mechanical damage at four depths where we have adequate bandwidths in the measured dipole dispersions.[18,19] Radial profiling of formation shear slowness can be used to estimate the radial extent of near-wellbore mechanical alteration or damage that helps in the completion strategy for optimal casing placement, design of perforation beyond the damaged annulus, and interpretation of potential permeability impairment. The near-wellbore mechanical damage characterized by radial profiling of formation shear slownesses can be correlated with the reservoir skin and productivity index. In addition to estimating the radial extent of mechanical alteration, the radial profiling algorithm yields an unambiguous estimate of the far-field formation shear slowness.

Figure 12 shows schematic diagram of a borehole in a formation subject to the maximum (S_H) and minimum (S_h) horizontal stresses. The presence of a borehole of radius *a* causes near-wellbore stress concentrations that result in both radially increasing and decreasing velocities away from the borehole surface in the maximum and minimum horizontal stress directions, respectively. The Backus-Gilbert inversion technique has been used to estimate the radially varying formation shear slowness from the measured borehole flexural dispersions for the fast and slow shear polarization azimuths. The inversion technique is based on a perturbation model that relates changes in the dispersion curve to changes in the effective formation material parameters.

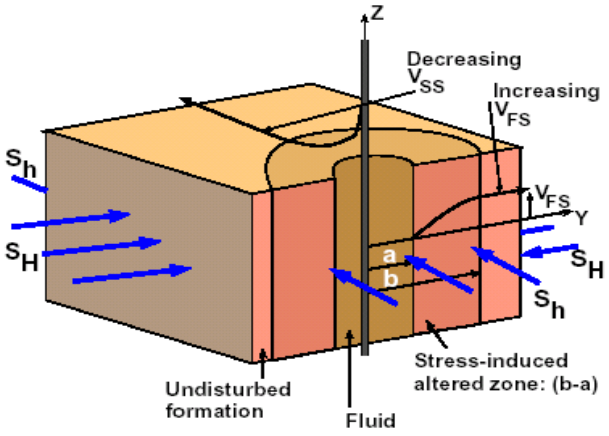

Fig. 12–Schematic diagram of a borehole of radius *a* in a formation subject to the maximum and minimum horizontal stresses. The stress-induced altered zone exhibits an increasing shear velocity away from the borehole surface at an azimuth parallel to the maximum horizontal stress and a decreasing velocity at an azimuth parallel to the minimum stress direction.

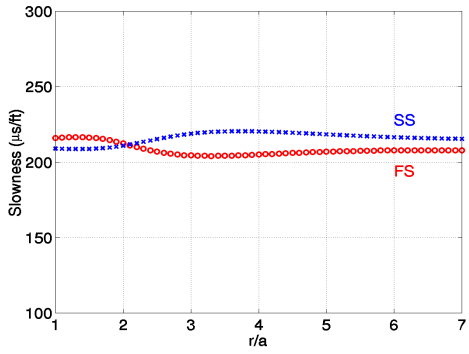

Fig. 13–Radial variation of the fast- and slow-shear slownesses along the maximum and minimum horizontal stress directions obtained from the dipole radial profiling algorithm.

Figure 13 displays inverted radial profiles of the formation fast-shear (FS) and slow- shear (SS) slownesses along the maximum and minimum horizontal stress azimuths at measured depth of 20,078.5 ft. Notice that the fast-shear slowness profile shown by red circles shows a reduction in the slowness over a radial distance of r/a = 2.5 to 5 before attaining the far-field shear slowness. In contrast, the slow-shear slowness profile shown by blue circles shows an increase in the slowness over the same radial distance.

To understand these radial profiles in the two orthogonal directions, we should examine the annular pressure history during surge and swab in the drilling process.[7,20]

A large annular pressure can push the formation out and introduce compaction up to a certain radial distance. A reduction in the annular pressure would allow the near-wellbore region to relax (reduce stress and increase observed shear slowness). If the rock were exhibiting plastic deformation, some of the past deformation history is captured during wireline logging and DRP results would show a slow increase in the shear slowness beyond this compacted annulus (which is somewhat faster than the far-field). Based on the near-wellbore stress distributions shown in Figs. 8a and 8b, it appears that an increase in the wellbore pressure causes more radial compaction along the maximum than that in the minimum horizontal stress direction.

Computational results for the radial variations of the fast and slow shear slownesses can also be obtained from the near-wellbore stress distributions shown in Figs. 8a and 8b, and the estimated stress coefficients of velocities (or slownesses) from the inverted formation nonlinear constants. The solid red and blue curves in Fig. 14 show the calculated radial variations in fast- and slow-shear slownesses, respectively, together with the inverted radial profiles (red and blue circles) obtained from the measured cross-dipole dispersions.

Note that the calculated radial profiles obtained from the near-wellbore stress distributions and stress-coefficients of slownesses are based on a theoretical model that does not assume any plastic deformation of the rock. Plastic deformation usually occurs close to the borehole surface. Thus, the compaction / relaxation history of the borehole may account for the differences between the inverted and predicted radial slowness profiles.

Changes to the radial profile may also be induced by invasion of drilling mud filtrate and / or mud particles. Near-borehole stiffening *could* be caused by the radial invasion of the monomer and resin materials used in the synthetic water-based mud to strengthen the weak sand reservoir. Conversely, invasion of mud filtrate resulting in a super-charging of the near-wellbore region might result in a softening of the formation. Inverted shear slowness profiles indicate the most significant alteration occurs within approximately 2xborehole diameters of the borehole surface. This is consistent with the estimated radial extent of penetration of the monomer/esin materials used in the Ursa-11 well.[1]

Figures 15, 16, and 17, respectively, show similar results for radial profiles of the fast- and slow-shear slownesses in the two orthogonal directions at measured depths of 20,540 ft in the depleted sand, and 20,599 and 20,685.5 ft in shale below the sand reservoir.

Summary and conclusion

Both the maximum and minimum horizontal stress magnitudes together with stress-coefficients of plane wave velocities have been estimated using multi-frequency inversion of cross-dipole dispersions. Inversion of borehole sonic data for the formation stress parameters is carried out by using sonic velocity variations caused by stress concentrations outside any mechanically altered annulus, such as that caused by plastic yielding or invasion of monomer or resin materials. We determine the radial extent of near-wellbore alteration that is not suitable for the inversion of sonic data for far-field stresses by comparing measured radial profiles of shear slownesses with that calculated using the near-wellbore stress distributions in the absence of any plastic yielding. Generally, we use only low-frequency sonic data that are less sensitive to near-wellbore mechanical alteration for estimating far-field stresses. This limits the use of cross-dipole dispersions to below the cross-over frequency for estimating stress parameters.

Minimum horizontal stress magnitudes were also estimated at two depths in shale from mini-frac tests using the dual- packer module of the MDT tool. At one of these depths, we have estimates of the minimum horizontal stress magnitude from both the inversion of cross-dipole dispersions and the MDT stress module. Reasonable agreement has been observed between the minimum horizontal stress magnitude obtained from these two techniques.

We have also analyzed cross-dipole dispersions to characterize near-wellbore alteration at select depths. The radial extent of near-wellbore alteration has been estimated using dipole radial profiling (DRP) of formation shear slowness along the two principal shear polarization directions. Radial profiles in the depleted sand (MD 20,540 ft), as well as at two other depths (MD 20,599 and 20,658.5 ft) in shale below it show clear evidence of plastic yielding in the potential breakout region. In addition, we have observed near-wellbore stiffening of the formation extending up to about 1 to 2 feet from the borehole surface. The stiffening of the rock may have been caused by invasion of the monomer and resin materials used in the drilling mud to mitigate the fluid loss in the presence of large overbalance.[1]

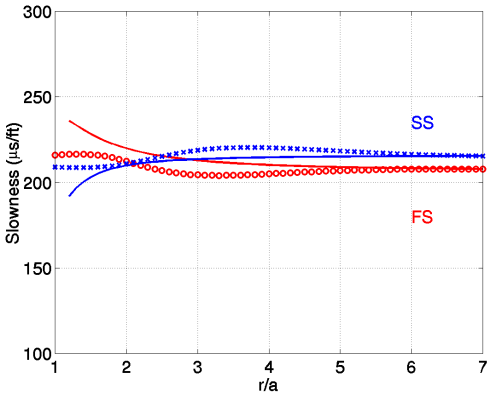

Fig. 14–MD 20,078.5 ft: Radial variation of the fast- and slow-shear slownesses along the maximum and minimum horizontal stress directions obtained from the inversion of cross-dipole dispersions. The solid red and blue curves are theoretical shear slowness variations obtained using the estimated stress-coefficients of slownesses and formation horizontal stresses.

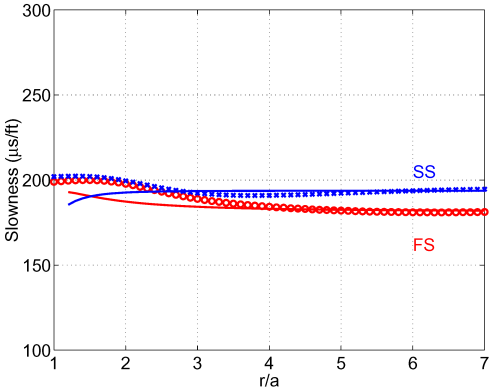

Fig. 15–MD 20,540 ft: Radial variation of the fast- and slow-shear slownesses along the maximum and minimum horizontal stress directions obtained from the inversion of cross-dipole dispersions. The solid red and blue curves are theoretical shear slowness variations obtained using the estimated stress-coefficients of slownesses and formation horizontal stresses.

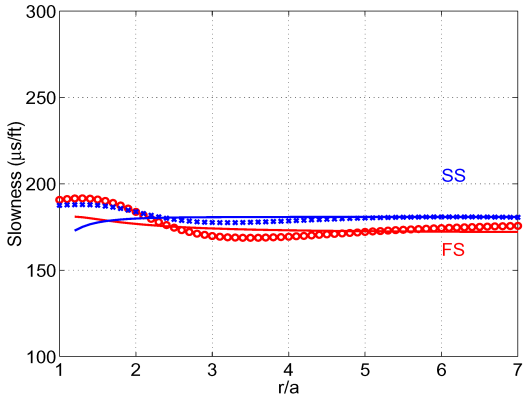

Fig. 16–MD 20,599 ft: Radial variation of the fast- and slow-shear slownesses along the maximum and minimum horizontal stress directions obtained from the inversion of cross-dipole dispersions. The solid red and blue curves are theoretical shear slowness variations obtained using the estimated stress-coefficients of slownesses and formation horizontal stresses.

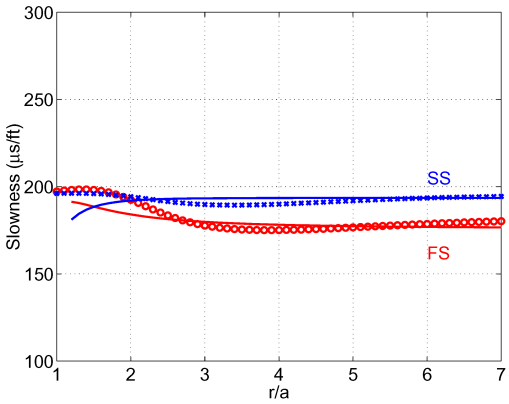

Fig. 17– MD 20,658.5 ft: Radial variation of the fast- and slow-shear slownesses along the maximum and minimum horizontal stress directions obtained from the inversion of cross-dipole dispersions. The solid red and blue curves are theoretical shear slowness variations obtained using the estimated stress-coefficients of slownesses and formation horizontal stresses.

Nomenclature

S_V	= Overburden stress
SHmax	= Maximum horizontal stress
Shmin	= Minimum horizontal stress
σ_{ij}	= Effective stress tensor
S_{ij}	= Formation stress tensor
P_P	= Pore pressure
P_W	= Wellbore pressure
α	= Biot parameter
δ_{ij}	= Kronecker delta
K	= Bulk modulus of the dry frame
K_S	= Bulk modulus of solid matrix
ϕ	= Porosity
a	= Borehole radius
f_i	= i-th frequency
V^F_m	= Fast flexural velocity at wavenumber k_m
V^S_m	= Slow flexural velocity at wavenumber k_m
C_{111}, C_{144}, C_{155}	= Formation nonlinear constants
L_{Mj}, M_{Mj}, N_{Mj}, P_{Mj}	= Sensitivity integrals
σ_1	= Maximum effective principal stress
σ_3	= Minimum effective principal stress
μ_f	= Coefficient of internal friction
σ_{rr}	= Effective radial stress
$\sigma_{\theta\theta}$	= Effective hoop stress
σ_{zz}	= Effective axial stress
NF	= Normal-fault stress regime
SS	= Strike-slip stress regime
RF	= Reverse-fault stress regime
MD	= Measured depth
TVD	= True vertical depth

Acknowledgements

We are grateful to our Shell colleagues Jim Wieseneck for useful comments on the manuscript and Jorge Lopez for support in obtaining publication permission. We thank the Ursa partnership (Shell, ExxonMobil, ConocoPhillips, BP), who own the data used in this work, for permission to publish this paper.

References

1. Van Oort, E., Gradishar, J., Ugueto, G., Cowan, K.M., Barton, K.K., and Dudley, J.W., "Accessing deep reservoirs by drilling severely depleted formations," SPE/IADC Drilling Conference, Amsterdam, The Netherlands, 19-21 February 2003 (SPE/IADC 79861).
2. Desroches, J., and Kurkjian, A., "Applications of Wireline Stress Measurements", SPE 48960 (1998).
3. Vernik, L., and Zoback, M.D., "Estimation of maximum horizontal principal stress magnitude from stress-induced well bore breakouts in the Cajon Pass Scientific Research Borehole," *J. Geophys. Res.*, **97**(B4), (1992) 5109-5119.
4. Gnirk, P. F., "The mechanical behavior of uncased wellbores situated in elastic/plastic media under hydrostatic stress", *J. Soc. Pet. Eng.*, (1972) 49-59.
5. Blakeman, E. R., "A case study of the effect of shale alteration on sonic transit time", Transactions, 23rd Annual Logging Symposium: SPWLA Paper II (1982).
6. Plona, T., Sinha, B., Kane, M., Shenoy, R., Bose, S., Walsh, J., Endo, T., Ikegami, T., and Skelton, O., "Mechanical damage detection and anisotropy evaluation using dipole sonic dispersion analysis", Transactions, 43rd Annual Logging Symposium, SPWLA, (2002) Japan.
7. Bratton, T., Bricout, V., Lam, R., Plona, T., Sinha, B., Tagbor, K., Venkitaraman, A., and Borbas, T., "Rock strength parameters from annular pressure while drilling and dipole sonic dispersion analysis", Transactions, 45th Annual Logging Symposium, SPWLA, Noordwijk, Norway, June 6-9 (2004).
8. Haimson, B.C., "*The Hydraulic Fracturing Method of Stress Measurement: Theory and Practice*", *Comprehensive Rock Engineering*, J. Hudson (ed.), Oxford, UK, Pergamon Press (1993), 3, 297328.
9. Sinha, B. K., "Inversion of borehole dispersions for formation stresses:", Proc. 1997 IEEE International Ultrasonics Symposium, pp. 781-786, IEEE Catalog No. 97CH36118 (October 5-8, 1997).
10. Sinha, B. K., Kane, M. R., and Frignet, B., "Case History – Dipole dispersion crossover and sonic logs in a limestone reservoir", *Geophysics*, **65**, (2000) 390-407.
11. Sinha, B.K., "Elastic waves in crystals under a bias", *Ferroelectrics,* **41**, (1982) 61-73.
12. Norris, A.N., Sinha, B.K., and Kostek, S., "Acoustoelasticity of solid/fluid composite systems", *Geophys. J. Internat.*, **118**, (1994) 439-446.
13. Sinha, B. K., Kane, M. R., Frignet, B., and Burridge, R., "Radial variations in cross-dipole slownesses in a limestone reservoir", 70th Ann. Internat. Mtg., Soc. Expl. Geophys., (2000) Expanded Abstract.
14. Nur, A., and Byerlee, J.D., "An exact effective stress law for elastic deformation of rock with fluids", *J. Geophys. Res.*, **76**, (1971) 6414-6419.
15. Walsh, J.B., 1965, The effect of cracks on the compressibility of rock, *J. Geophys. Res.,* 70(2), 381.
16. Moos, D., and Zoback, M.D., "Utilization of observations of well bore failure to constrain the orientation and magnitudes of crustal stresses: application to continental deep sea drilling project and ocean drilling program boreholes", *J. Geophys. Res.,* **95**, (1990) 9305-9325.
17. Jaeger, J.C., and Cook, N.G.W., "*Fundamentals of rock mechanics,"* ed., Third edition, (1979) New York: Chapman & Hall, pp. 28-30.
18. Burridge, R., and Sinha, B. K., "Inversion for formation shear modulus and radial depth of investigation using borehole flexural waves", 66th Ann. Internat. Mtg., Soc. Expl. Geophys., Expanded Abstract, (1996) 158-161.
19. Sinha, B. K., and Burridge, R., "Radial profiling of formation shear velocity from borehole flexural dispersions", Proc., 2001 IEEE International Ultrasonics Symposium, Atlanta, GA.
20. Bratton, T., Bornemann, T., Li, Q., Plumb, R., Rasmus, J., Krabbe, H., "Logging-while-drilling images for geomechanical, geological and petrophysical interpretations", Transactions, 40th Annual Logging Symposium, SPWLA (1999), Oslo, Norway, Paper JJJ.